Neuron
Article

Sun Compass Integration of Skylight Cues in Migratory Monarch Butterflies

Stanley Heinze[1] and Steven M. Reppert[1,*]
[1]Department of Neurobiology, University of Massachusetts Medical School, Worcester, MA 01605, USA
*Correspondence: steven.reppert@umassmed.edu
DOI 10.1016/j.neuron.2010.12.025

SUMMARY

Migrating monarch butterflies (*Danaus plexippus*) use a time-compensated sun compass to navigate from eastern North America to their overwintering grounds in central Mexico. Here we describe the neuronal layout of those aspects of the butterfly's central complex likely to establish part of the internal sun compass and find them highly homologous to those of the desert locust. Intracellular recordings from neurons in the monarch sun compass network reveal responses tuned to specific *E*-vector angles of polarized light, as well as azimuth-dependent responses to unpolarized light, independent of spectral composition. The neural responses to these two stimuli in individual neurons are mediated through different regions of the compound eye. Moreover, these dual responses are integrated to create a consistent representation of skylight cues in the sun compass throughout the day. The results advance our understanding of how ambiguous sensory signals are processed by the brain to elicit a robust behavioral response.

INTRODUCTION

Each fall, millions of monarch butterflies (*Danaus plexippus*) migrate from eastern North America to their overwintering grounds in central Mexico, some traveling distances approaching 4000 km. The yearly migration is one of the most astonishing and biologically intriguing phenomena in the animal world. Behavioral experiments have shown that the migrants use a time-compensated sun compass to maintain a southerly flight direction over the duration of the migration (Perez et al., 1997; Mouritsen and Frost, 2002; Froy et al., 2003). In general, this sun compass mechanism postulates that skylight cues, providing directional information, are sensed by the eyes and that this sensory information is then transmitted to a sun compass system in the central brain. There, information from both eyes is integrated and time compensated by the circadian clock so that flight direction is constantly adjusted to maintain a southerly bearing over the day. The monarch butterfly is an excellent model in which to study the time compensation process, because more is known about its circadian clock mechanism and clock cellular locations than in any other non-drosophilid insect (Reppert, 2007).

How are skylight cues used by migrating monarchs (Figure 1)? Flight simulator experiments have shown that the visibility of the outdoor sun, the most prominent light in the sky, is sufficient for proper orientation (Stalleicken et al., 2005). Moreover, other cues resulting from the scattering of sunlight, such as the pattern of polarized light and spectral gradients in the sky, also contain orientation information (Wehner, 2001; Coemans et al., 1994) (Figure 1A). As the electric field vectors of linearly polarized light (*E*-vectors) are arranged in concentric circles around the sun, they can indicate the sun's position, even when the sun itself is covered by clouds and only a small patch of blue sky is visible (Labhart, 1999). However, the symmetrical nature of skylight *E*-vectors leads to directional ambiguity unless they are integrated with the solar azimuth (the horizontal angular position of the sun) (Rossel et al., 1978; Pfeiffer and Homberg, 2007) (Figure 1A). For the detection of *E*-vector orientations, monarch butterflies, like most insects, possess a specialized dorsal rim area (DRA) of the compound eye (Reppert et al., 2004; Stalleicken et al., 2006; Labhart et al., 2009). Furthermore, monarchs were shown to respond to changes in the skylight polarization pattern with predictable changes in flight orientation (Reppert et al., 2004; Sauman et al., 2005), even though *E*-vector detection is not needed for proper orientation as long as the sun is visible (Stalleicken et al., 2005).

Although information about the central neuronal processing of skylight cues in the monarch brain has been lacking, a substantial amount of knowledge has been gathered about polarized light processing in the desert locust (*Schistocerca gregaria*). After *E*-vector detection in the locust DRA, information is passed through the optic lobe (Homberg and Paech, 2002; Homberg et al., 2003) and relayed through the anterior optic tubercle (AOTu) and two specialized regions of the lateral accessory lobes (LALs) (Pfeiffer et al., 2005). Information from both eyes is then integrated in the central complex (CC) (Vitzthum et al., 2002), a midline structure in the central brain. Within the CC, an array of neurons possess *E*-vector tunings that provide a topographical representation of the solar azimuth, such that the CC has emerged as the likely site of the insect sun compass (Heinze and Homberg, 2007). Spectral information appears to be integrated with *E*-vector information at an early stage of the locust brain, helping resolve the directional ambiguity inherent in the symmetrical nature of skylight *E*-vectors mentioned above (Kinoshita et al., 2007; Pfeiffer and Homberg, 2007). It is possible that a fundamentally similar integration mechanism for directionality also occurs in the monarch butterfly.

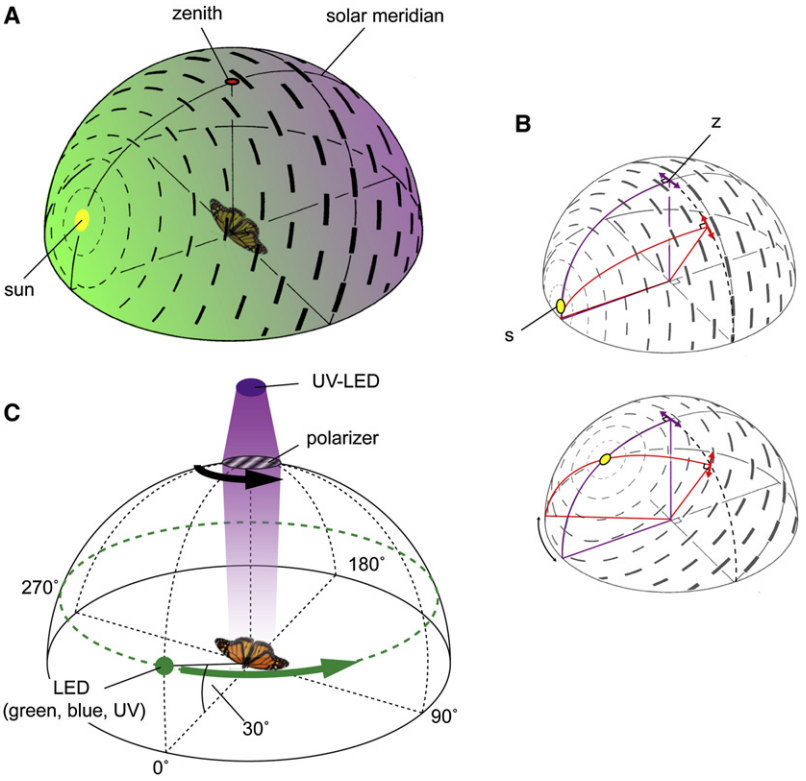

Figure 1. Skylight Cues and Their Study

(A) Patterns of polarized light and spectral gradients in the daylight sky. Black bars show *E*-vector orientation and degree of polarization (bar thickness) relative to the solar position (yellow circle) as seen by a migrating butterfly in the center of the celestial hemisphere. The skylight spectral gradient ranges from longer wavelength of light (green) dominating the solar hemisphere to shorter wavelengths (violet) in the antisolar hemisphere. Adapted from Wehner (1982).

(B) Polarization patterns in the sky at different solar elevations. Upper: When the sun (s) is near the horizon, observing the sky outside of the zenith (z) does not alter the 90° relationship between the solar azimuth and *E*-vector tuning; compare the direction of the bidirectional violet and red arrows. Lower: As solar elevation increases over the day, the relationship between the solar azimuth and *E*-vector tuning, as observed at a point outside the zenith, is more complex; compare the direction of the bidirectional violet and red arrows. The normal 90° relationship needs to be corrected by the difference between the intercept of the solar meridian on the horizon and the intercept of the red arc connecting the observed point through the sun to the horizon (bidirectional black arrow at the horizon). Adapted from Wehner (1982).

(C) Schematic illustration of simulated skylight cues applied as visual stimuli during intracellular recordings. Linearly polarized light in the ultraviolet (UV) range (violet) was presented from the zenith. The polarizer could be rotated through 360°, resulting in a rotating plane of polarization (*E*-vector). As a second stimulus, unpolarized light spots were presented at an elevation of ca. 30° in three different wavelengths (green, blue, UV). These light spots could be moved around the animal, passing through the entire azimuthal range of 360° at constant elevation. For both stimuli, LEDs were used as light sources. Azimuth of 0° was defined as the position directly in front of the animal, while the *E*-vector angle parallel to the body length axis of the butterfly was defined as 0° for polarized light stimuli. Stimuli were always applied sequentially and both clockwise and counterclockwise rotations (as seen by the animal) were tested.

To ultimately understand clock-compass interactions in monarchs, we have begun to anatomically and physiologically characterize the internal sun compass network in the butterfly, using the well-delineated sun compass network of the locust as a basis for comparison. Our results reveal the general layout of the neuronal machinery for sun compass navigation in the monarch brain, provide the first insights into a possible mechanism of integrating *E*-vector information and solar azimuth, and identify unique features of neuronal skylight sensing. More generally, the results address a fundamental problem of sensory processing by showing how seemingly contradictory skylight signals are integrated into a coherent, neural representation of the environment.

RESULTS

Anatomical Layout of the Sun Compass

To study the general anatomy of the monarch brain, we first performed three-dimensional reconstructions of the major brain neuropils. We labeled whole-brain preparations of the monarch with antibodies against the synaptic marker Synapsin, acquired confocal image stacks, and, based on these images, reconstructed the size and shape of identifiable brain regions. The resulting architecture of the monarch brain (Figures 2A–2C) was similar to that of other insect brains, with close resemblance to the brain of the hawkmoth *Manduca sexta*, the only other lepidopteran brain that has been examined in comparable detail (El Jundi et al., 2009).

In the monarch optic lobes, we identified and reconstructed the medulla, the lobula, the lobula plate, and the accessory medulla. In the central brain, we identified and reconstructed the central complex (CC), the anterior optic tubercles (AOTu), the antennal lobes, and the mushroom bodies (Figures 2A–2C). Because the present work focused on sun compass neuropils, the mushroom body lobes were not separated into their components; higher image resolution is required to resolve their compressed and intertwined organization.

The monarch AOTu, the first processing stage for sun compass information in the central brain of the locust (Pfeiffer et al., 2005), can be divided into three components: the large upper division, the lower division, and the nodular division, with its distinct, glomerular organization (Figure 2D). With the staining procedure used, the monarch LALs, the second relay stage for compass information in the locust brain, did not show distinct boundaries, consistent with the situation in the hawkmoth. However, the monarch LALs were defined on both sides of the CC using single-cell morphologies (Figures 3C, 3E, and 3G). Positioned posterior of the antennal lobe, they extended anteriorly, approximately from the depth of the lower division of the central body (CBL), until they almost reached the anterior

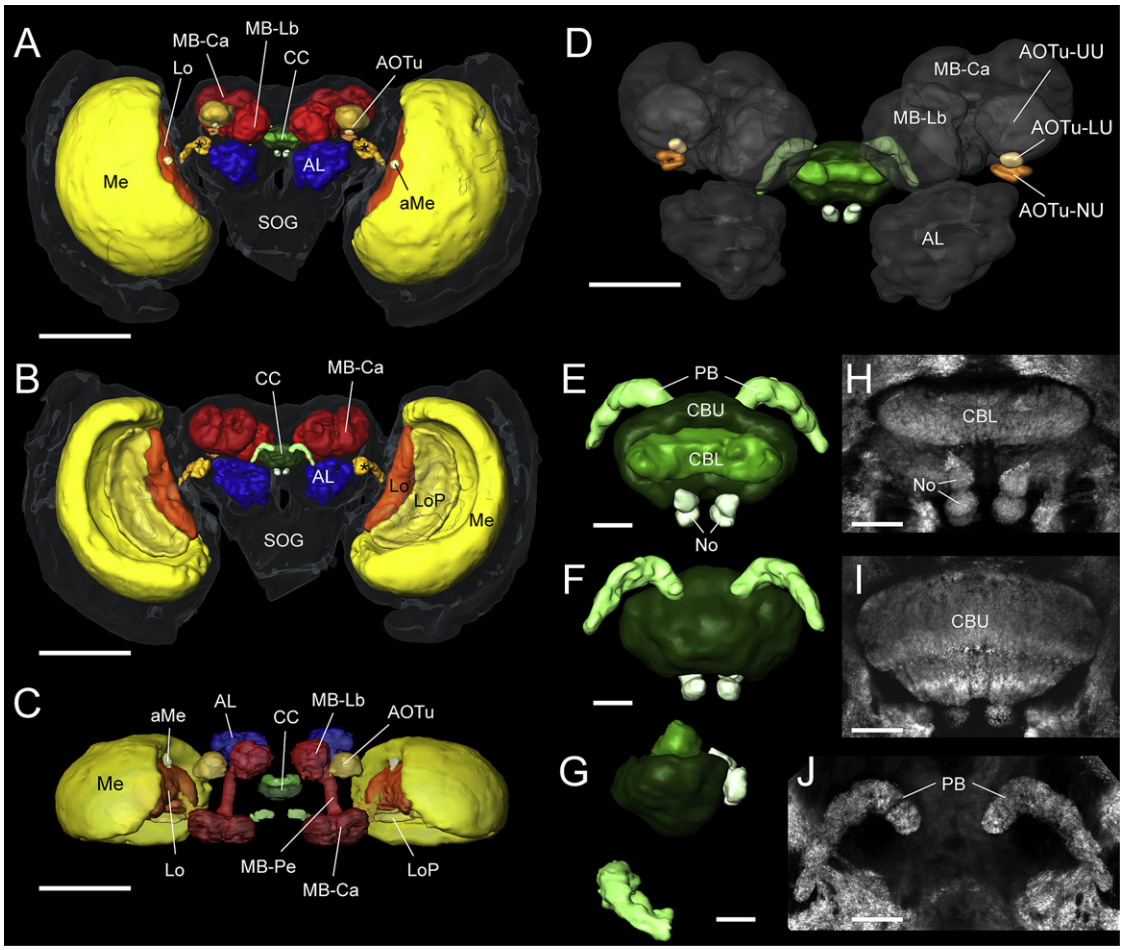

Figure 2. Anatomy of the Monarch Butterfly Brain

(A–C) Three-dimensional reconstruction of the brain of the monarch butterfly. Neuropils were reconstructed from confocal image stacks obtained from brains stained against synapsin. Shown are anterior view (A), posterior view (B), and dorsal view (C) (with respect to body axis). Dorsal side faces upward in (A) and (B), while the anterior side faces upward in (C). The transparent region surrounding the brain in (A) and (B) illustrates the boundaries of the brain. The asterisk indicates a yet unnamed brain region hitherto undescribed in insects, stretching from the lobula (Lo) of the optic lobe to the calyx of the mushroom body (MB-Ca).

(D) Anterior view of the proposed compass neuropils of the central brain. Shades of brown reveal the smaller subunits of the anterior optic tubercle (AOTu) in both brain hemispheres. Shades of green show the compartments of the midline-spanning central complex (CC).

(E–G) Anterior (E), posterior (F), and lateral (G) views of a three-dimensional reconstruction of the monarch CC. Neuropils were reconstructed from high-resolution confocal image stacks obtained from anti-synapsin-labeled brains.

(H–J) Maximal-intensity projections of confocal image stacks (frontal plane) from an anti-synapsin-labeled brain. Visible are the lower division of the central body (CBL) and the noduli (No) (H), the upper division of the central body (CBU) (I), and the protocerebral bridge (PB) (J).

aMe, accessory medulla; Me, medulla; LoP, lobula plate; AL, antennal lobe; MB-Lb, lobes of the mushroom body; MB-Pe, pedunculus of the mushroom body; SOG, suboesophageal ganglion; AOTu-UU, upper unit of the AOTu; AOTu-LU, lower unit of the AOTu; AOTu-No, nodular unit of the AOTu. Scale bars represent 500 μm (A–C), 200 μm (D), or 50 μm (E–J).

surface of the brain. Simultaneous dye-fills of multiple CBL-tangential neurons revealed a distinct neuropil region containing the postsynaptic endings of these cells (Figures 3A and 3B). Because of the typical, microglomerular shape of these endings, this neuropil region is probably the monarch homolog of the combined lateral triangle/medial olive areas of the locust (data not shown). Spatially, these areas were located on either side of the midline, between the LAL and the posterioventral surface of the mushroom body lobes, and slightly anterior to the CBL.

We next focused on the detailed reconstruction of the monarch CC, the proposed integration site of sun compass information in the insect brain. High-resolution confocal imaging revealed that the butterfly CC, as in other insect species, can be divided into four major components, the protocerebral bridge (PB), the upper division of the central body (CBU), the CBL, and the paired noduli (Figures 2E–2J). However, unlike in the locust brain, the orientation of the monarch CC and the remaining central brain were rotated by roughly 90° (around the sagittal axis), with respect to the fixed orientation of the optic lobes. Therefore, the monarch

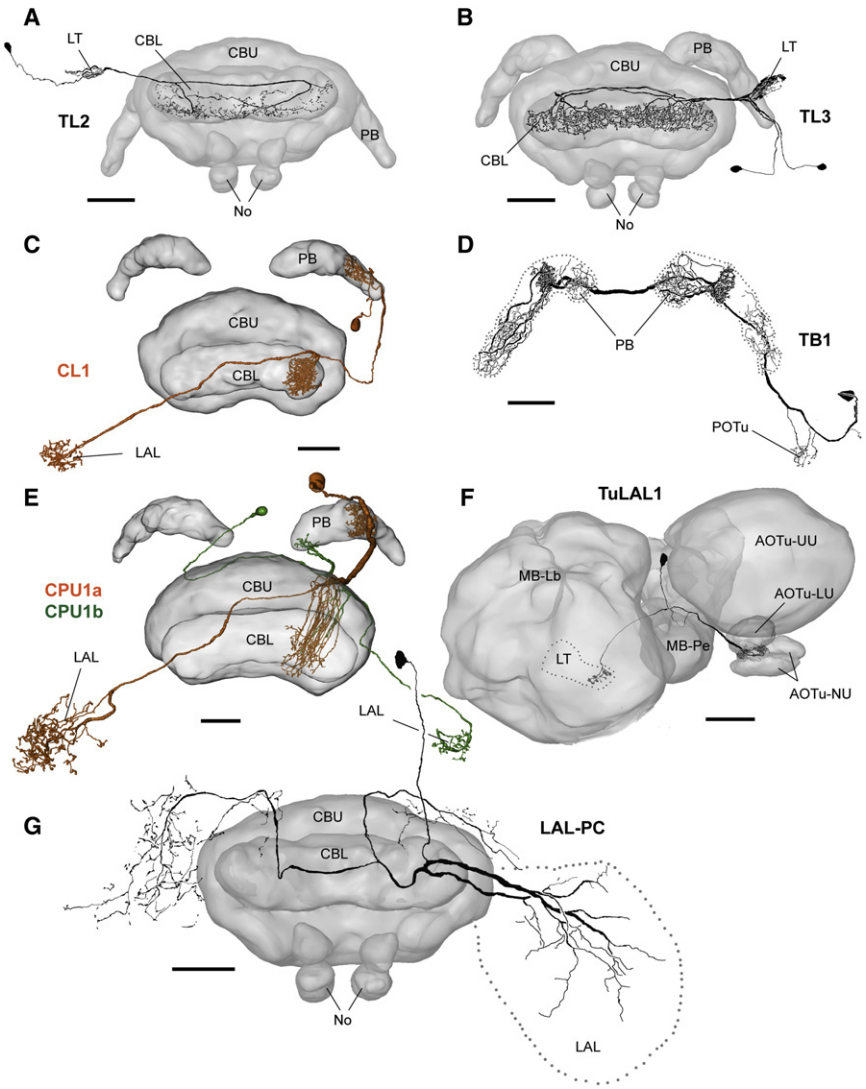

Figure 3. Neurons of the Proposed Monarch Butterfly Sun Compass Network

Reconstructions of dye-injected neurons at different levels of the compass network projected onto the three-dimensional reconstruction of the central complex (CC). Dye injections revealed several classes of neuron in the monarch brain directly homolog to neurons known to constitute the sun compass in the locust (*Schistocerca gregaria*). Shown are two-dimensional, frontal reconstructions projected onto a three-dimensional reconstruction of the central complex (CC) (A, B, D, F, G) or three-dimensional reconstructions of neurons with CC structures reconstructed from the same preparation (C and E).

(A and B) Tangential input neurons TL2 and TL3 connecting the lateral triangle (LT) to specific layers of the lower division of the central body (CBL).

(C) Anterodorsal view of a columnar cell type (CL1) connecting single columns of the CBL to single columns of the protocerebral bridge (PB) and a small region of the lateral accessory lobe (LAL).

(D) Tangential neuron TB1 connecting the PB to the posterior optic tubercle (POTu). Note the intricate pattern of varicose endings (likely output sites) and smooth endings (likely input sites) in different columns of the PB (outline of PB indicated by dotted line).

(E) Anterodorsal view of columnar neuron types CPU1a and CPU1b connecting single columns of the PB with columnar regions of the upper division of the central body (CBU) and large areas of the LAL. The CPU1b neuron was reconstructed from a separate preparation and had to be restricted to major arborizations because of superimposed staining from other neurons.

(F) Neuron type TuLAL1 providing input to the CC compass network. It connects the anterior optic tubercle (AOTu) to the LT, which lies directly posterior of the mushroom body lobes (MB-Lb).

(G) Neuron type LAL-PC potentially connecting the CC-output in the LAL to regions of the unstructured protocerebrum adjacent to the CC. On the ipsilateral side of the cell only major branches could be reconstructed due to superimposed staining from another neuron. Outline of the LAL is approximate only. AOTu-UU, upper unit of the AOTu; AOTu-LU, lower unit of the AOTu; AOTu-NU, nodular unit of the AOTu; No, noduli. Scale bars represent 50 μm. Neuron nomenclature (bold abbreviations) is adopted from the locust (Müller et al., 1997; Pfeiffer et al., 2005; Heinze and Homberg, 2007, 2008, 2009) (see Figure S1).

PB is located on the posterior side of the central body close to the posterior surface of the brain (Figures 2E–2G). The distinctly noncontinuous layout of two hemispheres of the monarch PB again resembled the situation in the hawkmoth. The central body and the PB were separated by a midline-spanning neuropil that left two gaps on either side for passage of the W-, X-, Y-, and Z-bundles. These massive tracts provide the only connection between the PB and central body and contain the axons of all compass-related columnar neurons of the CC. Within the central body, the bean-shaped CBL was located anterior to the larger CBU, while the noduli were located ventrally (Figure 2E).

Neurons within the Sun Compass Network

We reconstructed individual neurons of the monarch CC to further define the butterfly sun compass network and substantiate that the layout of this brain area is highly conserved between locusts and monarchs. Of the five groups of neuron (TL, CL1, TB, CPU1, CP) known to constitute the polarization vision network of the locust central complex (Heinze et al., 2009), we identified four groups in the monarch CC, covering all processing stages from the proposed input to the proposed output neurons of the CC (Figure 3; Table 1). Homologies were established based on detailed information regarding the location of input/output arborizations, the structure of terminals, and the heterolateral connectivity patterns (Figure S1 available online, Figure 3, Table 1). Consequently, we classified the identified neurons as monarch butterfly versions of TL2 (n = 6), TL3 (n = 5), CL1 (n = 4), TB1 (n = 4), CPU1a (n = 6), and CPU1b neurons (n = 1). Although subtypes of CL1 neurons could not be identified unambiguously in the monarch, CPU1 subtypes (CPU1a/b) could be clearly distinguished in monarchs because all arborizations of CPU1b neurons were located contralateral

Table 1. Morphology of Neuronal Cell Types Involved in Polarized Light Processing in the Locust and Their Monarch Butterfly Homologs

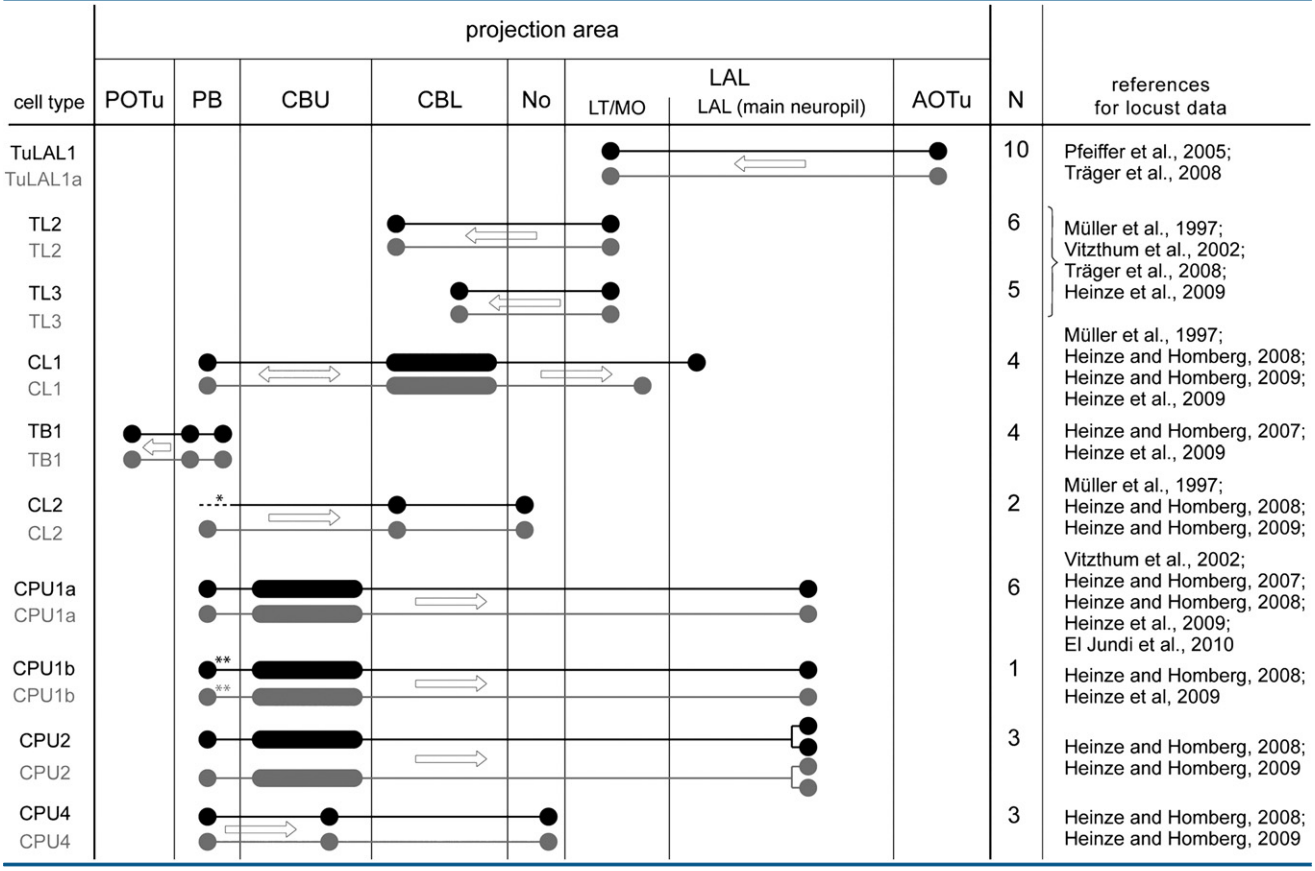

*Neurites could not be traced beyond the posterior chiasma (located between the central body and the protocerebral bridge).
**Arborizations in the protocerebral bridge are located contralateral to the soma.
Neurons from the monarch butterfly are drawn in black, while neurons from the desert locust are shown in gray. Filled circles indicate the location of arborization trees. In the CBU and CBL, arborization trees covering all layers within each column are shown as elongated circles. Bilateral arborizations in the LAL are indicated for CPU2 cells. Arrows indicate the proposed polarity of cells (Heinze and Homberg, 2008). Note that monarch butterfly counterparts for locust CP-neurons (Vitzthum et al., 2002; Heinze and Homberg, 2007, 2008; Heinze et al., 2009), TB2 cells (Heinze and Homberg, 2009; Heinze et al., 2009), and TuLAL1b cells (Pfeiffer et al., 2005, Pfeiffer and Homberg, 2007; Träger et al., 2008) have not been identified. Abbreviations: CBU, upper division of the central body; CBL, lower division of the central body; AOTu, anterior optic tubercle; LAL, lateral accessory lobe; LT, lateral triangle; MO, medial olive; No, noduli; PB, protocerebral bridge; POTu, posterior optic tubercle; N, number of reconstructions for each cell type. TuLAL, neuron connecting the AOTu to the LAL; TL, tangential cell of the CBL; CL, columnar cell of the CBL; TB, tangential cell of the PB; CPU, columnar cell of the PB and CBU.

to the soma (Figure 3E), which is the defining feature of locust CPU1b cells (Heinze and Homberg, 2008; Figure S1E). In addition to neurons of the core polarization-sensitive network, conditionally polarization-sensitive neurons of the locust provide another level of complexity to the CC-network, as they are thought to be recruited only in a context-dependent manner (Heinze and Homberg, 2009). Likewise, homologs of all three conditionally polarization-sensitive cell types were also identified in the monarch CC (CL2, CPU2, and CPU4) (Table 1). The only major types of neuron that were not found in the monarch were homologs of locust cells directly connecting the PB with the lateral triangle/medial olive (CP1, CP2).

Not only were the CC components of the polarization vision network largely conserved between the species, but the input and proposed output pathways were also comparable. On the input side, we could identify neurons connecting one of the small subunits of the AOTu with the lateral triangle of the LALs (TuLAL1; n = 10; Figure 3F, Table 1). On the output side, a characteristically shaped neuron was identified that connected large parts of the LAL with regions of the unstructured protocerebrum, located lateral and dorsal to the monarch central body (LAL-PC-neuron; n = 1; Figure 3G; Figure S1G).

Polarized Light Responses by Sun Compass Neurons

We next used intracellular recordings to examine the response properties of CC monarch neurons in the context of neural integration of the major skylight cues (polarized and unpolarized light stimuli). There were three considerations for evaluating these

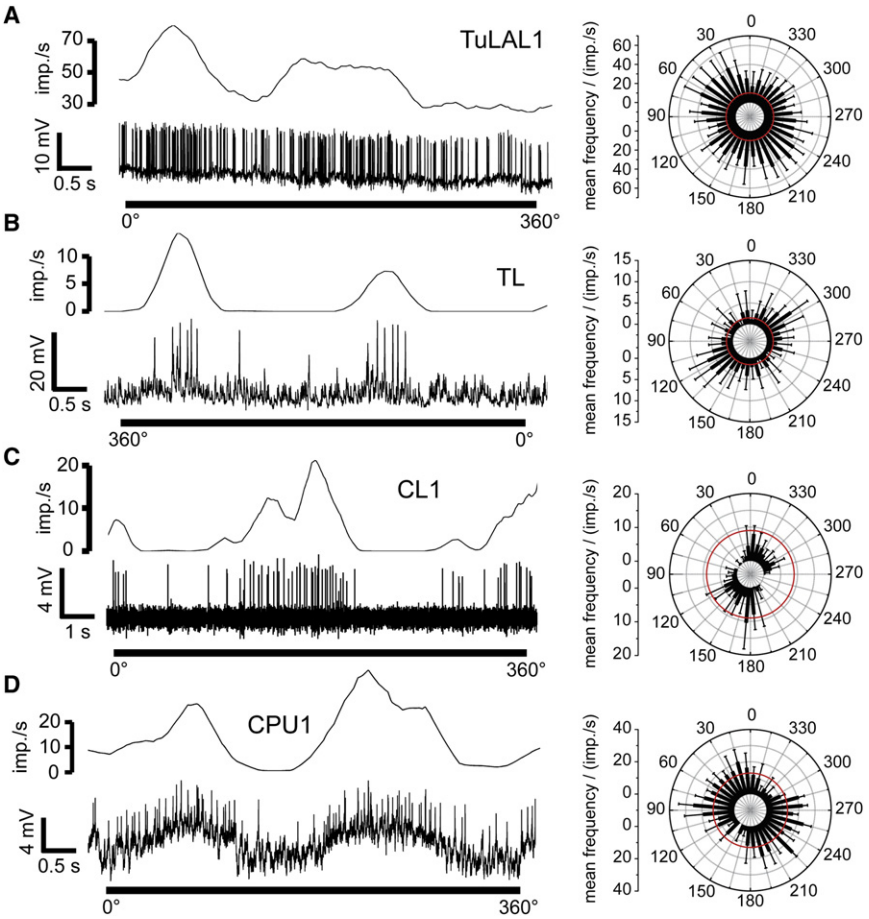

Figure 4. Polarized Light Responses by Neurons from the Monarch Brain

E-vector-dependent neuronal activity in a TuLAL1 neuron (A), a TL-type neuron (B), a CL1 neuron (C), and a CPU1 neuron (D). Left-hand panels show spike trains (lower traces) and mean frequency (upper traces) in response to one 360° rotation of the polarizer. Right-hand panels show the corresponding circular diagrams of mean spike frequency against the presented *E*-vector orientation during subsequent rotations of the polarizer (bin width 10°, mean ± SD). Red circles indicate background spike frequencies.

recordings. First, which skylight cues are actually processed by the monarch central brain? Second, how do monarchs resolve the directional ambiguity of skylight *E*-vectors (Figure 1A)—that is, do they use spectral gradients for distinguishing the solar and antisolar hemisphere, as suggested for locusts? The third issue was defining how polarized and unpolarized light responses are integrated to ensure that *E*-vector tuning actually provides an accurate reflection of the solar azimuth over the course of the day (Figures 1A and 1B).

For recordings, a migratory butterfly was mounted in the recording setup. Two types of visual stimuli (linear polarized light and unpolarized light spots) were applied during experimentation (Figure 1C). Prior to recordings, all migrants were housed in 11 hr of light and 13 hr of darkness, simulating outdoor lighting conditions at capture; physiological experiments were centered around Zeitgeber time (ZT) 5, which was 5 hr after lights-on, so that substantial variation in time-of-day of recording would not confound the results. Nonmigratory monarchs were used for initial recordings and some control experiments.

When presented with zenith-positioned polarized light in the UV range (365 nm), 33 neurons of the monarch brain responded with significant *E*-vector-dependent modulations of their spike frequency, as revealed by circular statistics ($p < 0.05$; Figure 4). Polarized UV light was used because the monarch DRA ommatidia only express a UV opsin (Sauman et al., 2005) and have been shown to be maximally sensitive to wavelengths below 380 nm (Stalleicken et al., 2006). Of the *E*-vector-responsive cells, 19 could be identified anatomically postrecording. All of these cells were components of the proposed polarization vision network described above. We identified seven TuLAL1 cells, six TL-type cells, two CL1 cells, an individual TB1 cell, and three CPU1 neurons; hence *E*-vector-dependent responses were present from the input stage of the polarization vision network (TuLAL1 cells) to the output stage of the CC (CPU1 cells).

Generally, each neuron showed a typical modulation of its spike frequency in response to changing *E*-vector angle, with maximal activity separated from minimal activity by 90° (Figure 4). Thus, each cell possessed a preferred *E*-vector orientation (Φ_{max} value). These Φ_{max} values differed between recordings but did not detectably differ between the *E*-vector rotation rates of 30°/s and 60°/s. As expected, most neurons showed polarization opponency; that is, they were always excited near their Φ_{max} value and inhibited near their Φ_{min} value (Figures 4B and 4D). As notable exceptions, four of the seven TuLAL1 neurons, together with one CPU1 neuron, showed excitation only (Figure 4A; maximum excitation at Φ_{max} and minimum excitation at Φ_{min}). This excitation response was correlated with strong bursting activity and a transient lights-on excitation in TuLAL1 cells. A solely inhibitory response was found in one CL1 neuron (Figure 4C).

For further physiological characterization, the response amplitude (R; a measure for the amount of frequency modulation during the response) was calculated for each recording. The strongest responses could be found in TuLAL1 neurons, which on average responded four times stronger than TL-type neurons. Despite their weak response amplitude and low activity as revealed by spikes, four of the six TL neurons showed strong modulations of sub-threshold activity in response to the rotating *E*-vector. Finally, both CL1 cells, as well as the single TB cell, behaved similarly to TL neurons, while the CPU1 recordings possessed R values between TL and TuLAL1 cells.

These physiological characteristics, together with the location of the recording site in the brain and responses to unpolarized light (see below), allowed us to assign cell types to the majority of the anatomically unidentified recordings. For all recordings from migratory monarchs, this led to a combined number of 13 TuLAL1 neurons, seven TL-type neurons, one CL1 neuron, and one CPU1 neuron, while five recordings remained unallocated due to ambiguous characteristics. Overall, only one anatomically identified TuLAL1 and one TL neuron did not respond significantly to our polarized light stimuli. This might have been due to the zenithal stimulation's being outside the neuron's receptive field or to interindividual variability in response characteristics.

Azimuth-Dependent Responses to Unpolarized Light by Sun Compass Neurons

While in the recording setup, the same 27 neurons tested for polarized light responses in migrants were also examined for responses to unpolarized light. Specifically, small unpolarized light spots were moved around the animal at a rotation velocity of either 30°/s or 60°/s and at constant elevation (ca. 30°) passing through the entire azimuthal range of 360° (Figure 1C). Three distinct wavelengths were used for the experiments, green (530 nm), blue (470 nm), and UV (365 nm). These wavelengths of unpolarized light were used because they represent the range of wavelengths comprising the spectral gradient in the daylight sky—from longer wavelengths dominating the solar hemisphere to shorter wavelengths dominating the antisolar hemisphere (Figure 1A). Green stimuli were tested in all recordings, whereas UV stimuli were tested in 19 recordings and blue stimuli in ten recordings.

In total, 26 of the 27 cells responded to at least one of the three unpolarized light spots with a significant, azimuth-dependent modulation of spike frequency ($p < 0.05$), including the two cells without *E*-vector response. Of the 19 neurons presented with more than one wavelength, only three did not respond to all presented stimuli; among these, one did not respond to any stimulus, one did not respond to green, and one did not respond to UV. Generally, strong excitation was found for specific stimulus positions in one narrow azimuthal range, while stimulus positions at the opposite side (180° difference) lead to either no response or inhibition (Figure 5). Importantly, no significant difference in azimuthal tuning was apparent when comparing responses to the different wavelengths of unpolarized light within each cell (mean differences: green to UV: 23°; green to blue: 9°; blue to UV: 15°; see below). Exceptionally strong excitations could be observed in TuLAL1 neurons, in which peak, instantaneous frequencies regularly reached 200 impulses per second at their preferred azimuth. These neurons also showed the most consistent behavior, as all tested stimuli elicited a strong, significant response. In contrast, but consistent with the weak response to polarized light, the TL-type neuronal responses to unpolarized light were weaker and more variable. Of the six TL neurons tested with more than one wavelength, two did not show a significant response to at least one wavelength. Finally, the CL1 and CPU1 neurons both possessed a significant, azimuth-dependent response to the unpolarized stimuli (Figures 5G–5J). Taken together, the wavelength independence of responses suggests that monarchs use the solar azimuth itself for directional information, rather than skylight spectral gradients.

Differential Skylight Responses in Individual Neurons Are Mediated by Different Regions of the Monarch Eye

After establishing that neurons in the monarch brain have the capacity to respond to polarized and unpolarized light stimuli, we examined whether different regions of the compound eye mediate these responses. As polarized light is probably perceived by the DRA, we shielded the dorsal part of the compound eye, including the DRA, during sequential stimulation with rotating *E*-vectors and unpolarized, green light spots. Indeed, responses to polarized light were completely abolished during stimulation when the dorsal part of the eye was shielded (TuLAL1 cells, $n = 6$; compare Figures 6A and 6B), whereas, in the same neurons, responses to the green light spot were unaffected (TuLAL1 cells, $n = 5$; Figures 6C and 6D). For statistical analysis, response amplitudes for the different stimulus situations were normalized to the response of each cell when the eye was unshielded. These quantifications confirmed that neural responses to the green light spot were unaffected by shielding ($p = 0.1487$; Figure 6E), while the neuronal responses to polarized light were blocked, with response amplitudes indistinguishable from background activity ($p = 0.4483$; Figure 6F). Furthermore, unpolarized UV light presented from the zenith to unshielded eyes did not result in neuronal response amplitudes above background level over the 360° of rotation (Figure S2), underscoring the hypothesis that indeed changing *E*-vectors cause the observed frequency modulations in response to polarized UV light from zenithal stimulation.

Although many insects have a DRA that is anatomically and functionally distinct from the other regions of the retina (Labhart and Meyer, 1999), our results are unique in that they show that the dorsal eye is not required for mediating the azimuth-dependent responses in single neurons to unpolarized light spots but is essential for zenithal *E*-vector responses. Thus, skylight orientation information from two distinct regions of the compound eye is integrated in the individually recorded neurons—the dorsal eye (including the DRA) for polarized UV light responses and the laterally directed main retina for unpolarized light responses. It remains possible that polarized colored light spots presented to the lateral retina of monarchs can also elicit neuronal responses (Kelber, 1999), but this issue could not be examined given the constraints of our recording system. However, intracellular recordings of photoreceptors in the other regions of the monarch retina show low polarization sensitivity compared to the high sensitivity found in the DRA (Stalleicken et al., 2006).

Integration of Polarized and Unpolarized Light Responses

After describing the response characteristics of neurons to individual compass-related stimuli (polarized and unpolarized light), we analyzed the relation between *E*-vector tuning and azimuth tuning for the recorded cells from migratory monarchs. The expectation was that there would be a 90° difference between *E*-vector tuning and azimuth tuning within individual neurons, because polarized light was applied from the zenith (Wehner and Labhart, 2006) (Figures 1A and 1B).

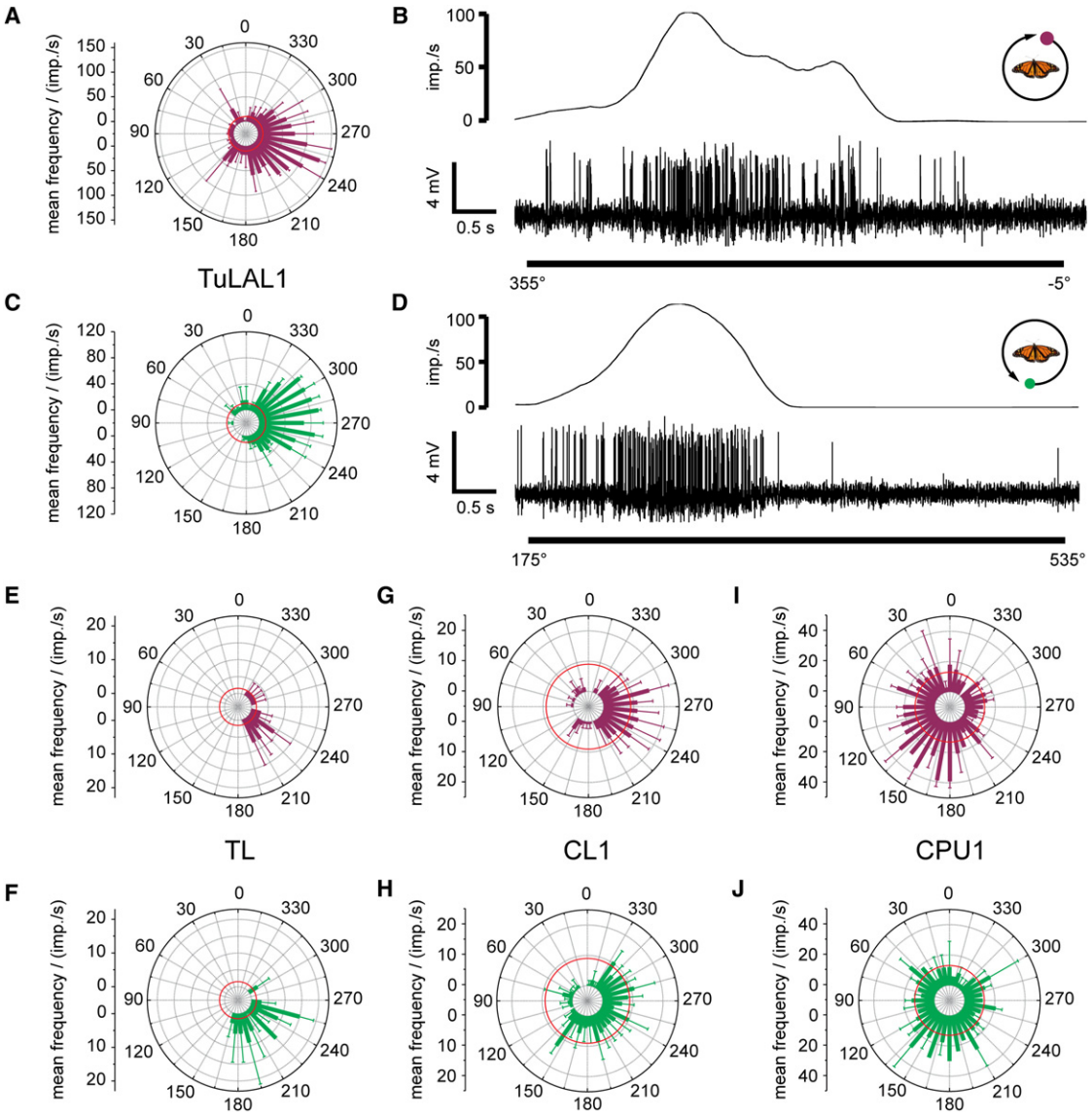

Figure 5. Azimuth-Dependent Responses to Unpolarized Light by Monarch Polarization-Sensitive Neurons

(A–D) Responses of a TuLAL1 neuron. (A and C) Circular diagrams of mean firing frequency plotted against the azimuthal position of the stimulus, for stimulations with a ultraviolet light spot (A) and a green light spot (C). (B and D) Spike trains (lower traces) and mean spike frequency (upper traces) of the neuronal responses shown in (A) and (C) during one 360° azimuthal revolution of the stimulus. (B) shows the response to a counter clockwise movement of an ultraviolet light spot, while (D) shows the response to a clockwise movement of a green light spot. Note that the starting positions for the two colors are located at opposite azimuth positions.

(E–J) Circular diagrams of responses in a TL neuron (E and F), a CL1 neuron (G and H), and a CPU1 neuron (I and J) to stimulation with ultraviolet light (E, G, and I) or green light (F, H, and J). For all circular diagrams, bin width was 10°, and the data are plotted as mean ± SD. Red circles indicate background spike frequencies.

As described above, the azimuth tuning in response to unpolarized colored light spots was independent of the stimulation wavelength used. Accordingly, when considering all neurons recorded from the vicinity of the left LAL (i.e., excluding the two later stage neurons from the PB), the absolute azimuth tunings for all unpolarized light responses were tightly clustered (Figures 7A–7C). Of the 24 neurons responding to unpolarized light spots, 22 exhibited azimuth tunings on the right side of the animal (256° ± 13.5°, mean ± standard deviation [SD]). Surprisingly, there was great variability of *E*-vector tunings in these cells, such that no clear common tuning angle was observed (n = 23) (Figures 7D and 7E). Moreover, there was no correlation between the *E*-vector tuning and azimuth tuning within individual neurons, as revealed by the analysis of the difference angles between the two tunings ($\Delta\Phi_{max}$ values). Virtually every value within the possible $\Delta\Phi_{max}$-range of 90° could be observed (Figure 7F), and the distribution of these values did not differ from a uniform distribution ($p > 0.15$).

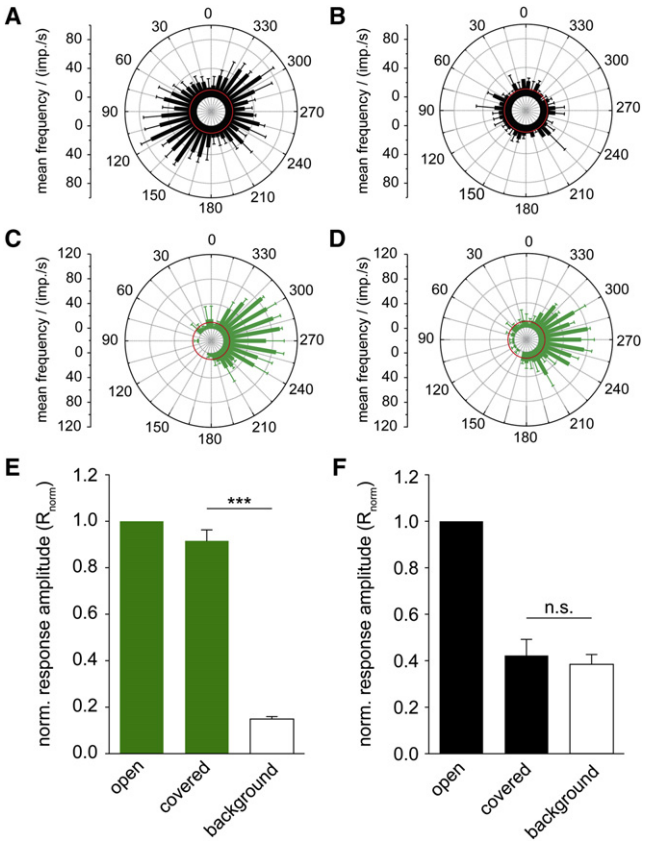

Figure 6. Differential Skylight Responses Are Mediated by Different Parts of the Monarch Eye

(A and B) Circular diagrams of mean spike frequency plotted against the presented *E*-vector orientation. Neuronal response before shielding (A) or during shielding of the dorsal part of the eye (B).

(C and D) Circular diagrams of mean spike frequency plotted against the azimuthal position of an unpolarized green light spot before shielding (C) or during shielding of the dorsal part of the eye (D).

(A)–(D) depict data from the same neuron. For all circular diagrams, the bin width was 10°, and the data are plotted as mean ± SD. Red circles indicate resting spike frequency.

(E and F) Comparison of mean normalized response amplitudes (R_{norm}) between the different experimental conditions (open, unshielded eye; covered, shielded eye; background, no stimulation). Values were normalized to the response amplitude of the unshielded condition and plotted as mean ± SE. (E) Responses to green light spots (n = 5 cells for each treatment). The covered condition could not be distinguished from the unshielded condition ($p = 0.1487$, two-tailed one-sample t test against hypothetical mean of 1), but a significant difference was present between the covered condition and background ($p < 0.0001$, two-tailed, paired t test). (F) Responses to *E*-vector orientation (n = 6 cells for each treatment). The covered condition was not significantly different from background activity ($p = 0.4483$) but showed a highly significant difference to the unshielded condition ($p = 0.0004$). Note that all neurons in (E) are also included in (F).

We next examined whether the large variability of *E*-vector tunings could be related to the different neuron types. Of the 25 neurons recorded from the left LAL, 22 responded to both polarized and unpolarized light, of which 13 could be classified as TuLAL1 neurons, five could be classified as TL-type neurons, and four remained unassigned to a particular neuronal type. Comparison of *E*-vector tuning and azimuth tuning showed no significant difference between these three groups of neuron (Figure S3; $p > 0.3$). Accordingly, distributions of $\Delta\Phi_{max}$ values for none of the groups deviated from a uniform distribution (Figure S3; $p > 0.05$). Thus neuronal cell type could not explain the variability of the *E*-vector tuning. The variability could be explained, as detailed below, by taking into account the daily changes in solar elevation and the region of the sky observed by the monarch DRA.

Modeling Time-Dependent Adjustment of *E*-Vector Tunings

For any sky point outside the solar meridian, the relation between the *E*-vector angle and the solar azimuth is complex and depends on the location of the observed point in the sky and the solar elevation (Figure 1B). As solar elevation changes over the day, the *E*-vector tuning of neurons not looking directly at the zenith needs continuous adjustment to provide consistent azimuthal information (Pfeiffer and Homberg, 2007).

The expected $\Delta\Phi_{max}$ value of 90° for polarized light stimulation from the zenith did not match the high variability and calculated average $\Delta\Phi_{max}$ value of 35° of recorded neurons in our studies. However, the variable $\Delta\Phi_{max}$ values we found in monarchs were similar to those from the AOTu neurons of the locust (Pfeiffer and Homberg, 2007). The locust data were explained by modeling the *E*-vector angle in the lateral center of the assumed receptive fields of the locust DRA over the course of the day (Pfeiffer and Homberg, 2007). Because of the different anatomical layout of the monarch DRA, however, the locust model cannot explain the observed *E*-vector tuning in monarchs. The locust DRA has a receptive field laterally centered at 60° elevation, while the monarch DRA receptive field is laterally centered at 80° elevation (Homberg and Paech, 2002; Stalleicken et al., 2006). As *E*-vector angles near the zenith only change marginally over the course of the day, the monarch $\Delta\Phi_{max}$ values predicted by the locust model are large (79° for the average recording time) (Figure 8A).

Across the entire monarch DRA, ommatidia are directed toward a narrow band of sky along the longitudinal axis of the butterfly, reaching from the apex (90°) down to elevations of 20°, restricting their view to the celestial hemisphere in front of the animal (Stalleicken et al., 2006; Labhart et al., 2009) (Figure 8B). As the majority of our recorded neurons were activated as though the sun is located on the right side of the animal (solar azimuth designated 0°), these neurons must be maximally excited by *E*-vectors along the 90° perpendicular axis in the sky (Figure 8B). To provide consistent compass information, *E*-vector information from the relevant part of the sky (90° axis, 20°–90° elevation) has to match the neuronal $\Delta\Phi_{max}$ values (absolute Φ_{max} values normalized to the azimuth tuning). Importantly, polarized light information in this sky region changes with increasing solar elevation, as a result of the decreasing angular distance between the observed points and the sun (Figure 1B; Figure S4).

Because the DRA is exposed to a mixture of different *E*-vector angles at all times, we calculated the average perceived *E*-vector (Figure 8C). Thereby, the contribution of individual *E*-vectors was weighted, based on the associated degree of polarization at the

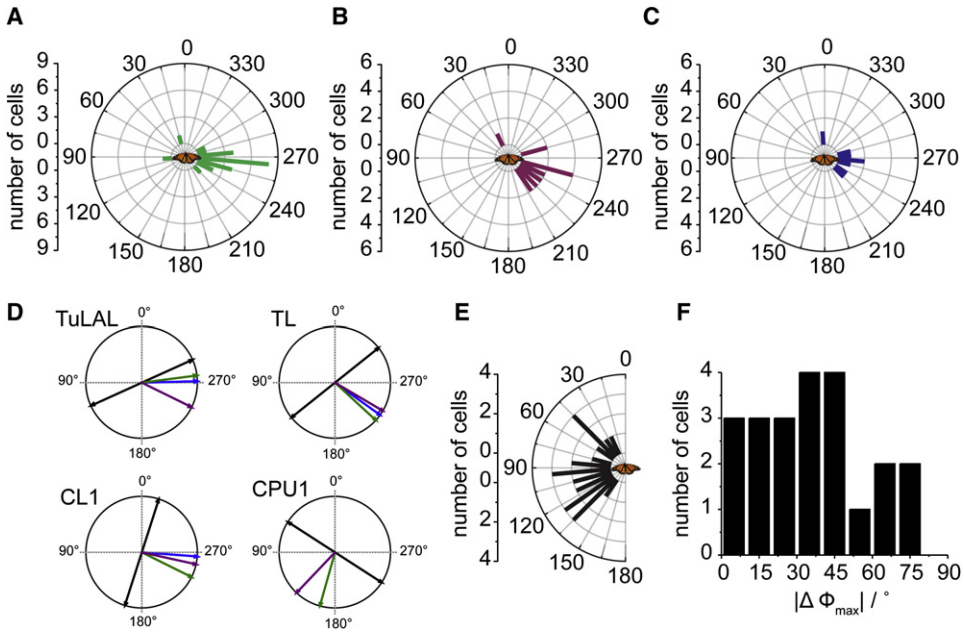

Figure 7. Relationship between *E*-Vector Tuning and Azimuth Tuning

(A–C) Circular distributions of preferred azimuth angles of all neurons recorded from the vicinity of the left lateral accessory lobe for unpolarized green light (A) (n = 23), an ultraviolet (UV) light (B) (n = 15), and blue light (C) (n = 8). All three distributions are significantly different from uniform distributions (green: 265° ± 35°, $p = 7.9 \times 10^{-8}$; UV: 248° ± 36°, $p = 3.2 \times 10^{-6}$; blue: 266° ± 39°, p = 0.003; Rayleigh test for circular data, mean ± SD).

(D) Tuning directions of individual neurons of different types (TuLAL, TL, CL1, and CPU1). Black bidirectional arrows indicate *E*-vector tuning (Φ_{max} values), whereas green, blue, and violet (UV) arrows indicate the preferred azimuth directions for the respective stimulation wavelengths.

(E) Distribution of Φ_{max} values of all neurons recorded from the vicinity of the left lateral accessory lobe (n = 23). The values show a broad mean orientation of 100° ± 39° (mean ± SD; Rayleigh test for axial data, p = 0.025).

(F) Distribution of difference angles between *E*-vector tuning and mean azimuth tuning ($\Delta\Phi_{max}$ values) within the possible range of 90°. The distribution is not different from a uniform distribution (Kuiper's V test for axial data, data set was tested after transformation to fit the 180° range of axial data, p > 0.15).

observed sky-point (Figure S4). As the solar elevation changes predictably over the day, we calculated the mean perceived *E*-vector as a function of daytime for the date and location the migratory monarchs were captured (the last configuration of skylight cues they have experienced) (Figure 8D). Indeed, the mean $\Delta\Phi_{max}$ value (29°) predicted with this function for the average recording time (ZT 5.4) closely matches the mean of the experimental data for monarchs (35°; p = 0.217) (Figure 8A). Furthermore, the model predicts increasing $\Delta\Phi_{max}$ values at earlier and later times during the day. In fact, retrospective analysis of variation in recording times around ZT 5 was consistent with time-dependent changes for *E*-vector tuning (Figure S5). Overall, our data suggest that time-dependent adjustment of *E*-vector tunings provides a consistent representation of solar azimuth in the monarch sun compass over the course of the day.

DISCUSSION

In the current studies, we have begun to unravel the anatomical and physiological properties of the essential sun compass system in migratory monarch butterflies. The results provide a new synthesis of the navigational capabilities of migrating monarchs, which includes describing the structural similarity and functional equivalence between the locust and monarch sun compass network, defining how migrating monarchs integrate skylight cues for directional information, and proposing two distinct clock-compass interactions necessary for migration.

Structural Similarity and Functional Equivalence

We have shown that the central brain of the monarch butterfly contains all the brain regions associated with sun compass navigation in other species (Homberg, 2004; Sakura et al., 2008). These include the AOTu, the lateral triangle, the LAL, and all compartments of the CC. These homologies, particularly between the monarch butterfly and the desert locust, could be extended to the level of single neuronal cell types and subtypes (Table 1; Figure 3). Furthermore, the comparison of the distribution of pre- and postsynaptic endings within single cell types suggests highly similar patterns of connectivity, especially in specialized elements of the CC-polarization-vision network (TB1 and CL1 neurons; Heinze and Homberg, 2007, 2009).

Consistent with this high degree of conserved morphology, the examined neuronal elements in monarch butterflies were found to serve similar functions as in the well-studied desert locust. However, there are some notable differences specific to the monarch, as discussed below. In general, we were able to show striking functional homology between the monarch butterfly and desert locust for neurons of the polarization vision pathway. The capacity for *E*-vector coding could be shown by

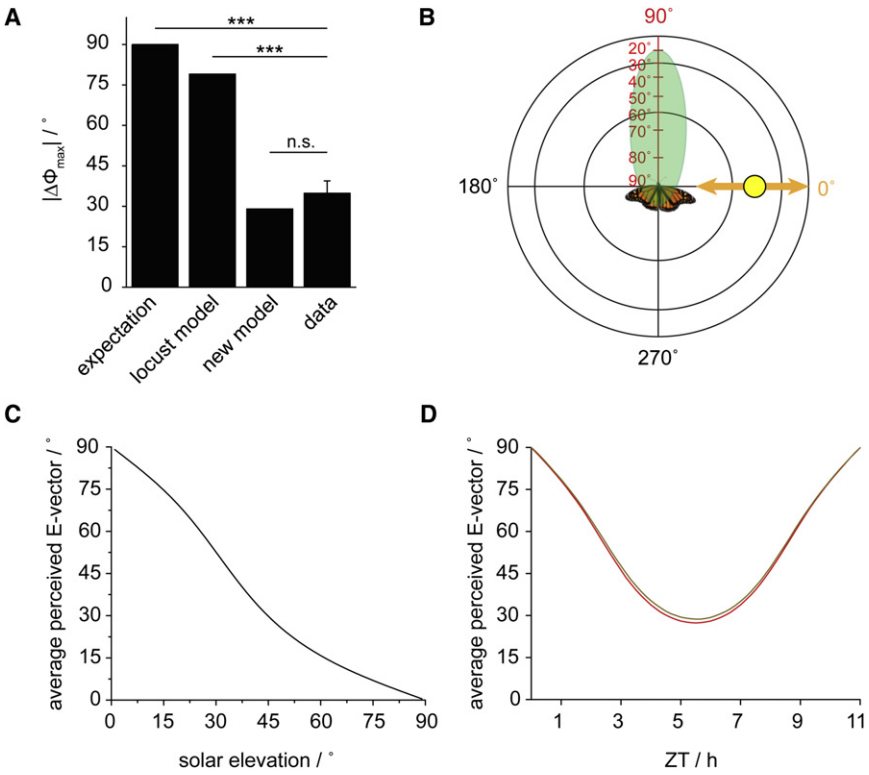

Figure 8. Modeling Time-Dependent Adjustment of *E*-Vector Tunings

(A) Comparison of various mean $\Delta\Phi_{max}$ values predicted for the average recording time (ZT 5.4). The original expectation for zenithal *E*-vector stimulation (90°, first bar) is shown with the prediction from the locust model (79°, second bar, Pfeiffer and Homberg, 2007; modified for geographical location of Texas and observed solar elevation of 80°), the prediction from the new model (29°, third bar), and the mean (± SE) of the $\Delta\Phi_{max}$ values of the data (mean = 35°, fourth bar). ***$p < 0.001$, using a one-sample t test against the predicted means; n.s., not significant.

(B) Illustration of the sky region used for calculating the average perceived *E*-vector. Coordinates on the sky use the sun as reference point (solar azimuth designated 0°). As examined neurons appear to be optimized for solar azimuth values on the right side of the animal, the region perceived by the DRA (transparent green oval) at the preferred *E*-vector angles must coincide with the perpendicular 90° axis on the sky. The different points of observation used for calculating relevant skylight parameters are indicated along the 90° axis. See also Figure S3.

(C) Average perceived *E*-vector for different solar elevations. This value is an estimate of the integrated *E*-vector information relayed from the monarch DRA. See also Figure S3.

(D) Average perceived *E*-vectors over the course of the day at the time and location of capture of the migratory butterflies. See also Figure S4. (Red line: Port Lavaca, Texas [latitude 28°37′N, longitude 96°37′W], 31st Oct.; yellow line: St. Marks's Wildlife Refuge, Tallahassee, Florida [30°26′N, 84°16′ W], 29th Oct.). Sunrise was set as ZT 0.

intracellular recordings for all processing stages in the monarch central brain, from early-stage neurons of the AOTu (Pfeiffer et al., 2005) to proposed output neurons of the CC (Heinze et al., 2009). Taking into account that butterflies and locusts are distantly related (lepidopterans and orthopterans diverged from each other circa 350–380 million years ago; Gaunt and Miles, 2002), this conservation of the polarization vision pathway is remarkable and suggests that the presence of a homologous, sophisticated sun compass network is a common feature in many insects.

How Migrating Monarchs Integrate Skylight Cues for Directional Information

In the desert locust, the spectral gradient in the sky is integrated with *E*-vector information to obtain a robust (unambiguous) compass signal. Importantly, our data from monarch butterflies show no such wavelength-dependent response in polarization-sensitive neurons despite their structural homology with locust polarization-sensitive neurons. All presented unpolarized light spots lead to strong excitatory responses in the same azimuth position, independently of the wavelength presented (green, blue, or UV). Thus these neurons respond to the azimuth position of the brightest source of light, which outdoors would be the sun itself, and which is integrated with *E*-vector information to obtain an unambiguous sun compass signal in monarchs. The monarch responses to unpolarized light spots were generally more pronounced than the responses to polarized light. This is an important finding and is consistent with flight simulator data showing that monarch butterflies have the capacity to use skylight polarization but utilize the sun as the prime source of directional information (Mouritsen and Frost, 2002; Froy et al., 2003; Reppert et al., 2004; Sauman et al., 2005; Stalleicken et al., 2005; Zhu et al., 2009).

But what about on cloudy days, when the view of the sun is blocked? Our modeling of the $\Delta\Phi_{max}$ values between *E*-vector and azimuthal tuning in recorded neurons suggests that there is a time-dependent adjustment of *E*-vector tuning with changing solar elevation over the course of the day, allowing *E*-vectors to provide an accurate representation of the solar azimuth, even though the sun itself cannot be seen. This process in the monarch appears to be remarkably similar to that first described in the locust (Pfeiffer and Homberg, 2007), suggesting that anticipation of changing skylight information by adjusting *E*-vector tuning is a fundamental feature in insects that use a sun compass for directional information. Although fundamentally similar in terms of outcome (*E*-vectors providing a reliable representation of solar azimuth) the details of the elevation compensation mechanism differ. Specifically, the compensation mechanism in monarchs and locusts seems to be optimized for the difference in DRA architecture between both species, which dictates the region of the sky observed by the DRA. We further propose that elevation compensation involves use of the circadian clock to track solar elevation changes over the course of the day. The use of a clock could explain how polarized and

unpolarized light stimuli are properly integrated at the level of a single neuron, even though the stimuli are processed in separate pathways.

The Migratory Monarch as a Model of Clock-Compass Interactions

For migrating monarchs to maintain a constant flight bearing over the day, they need a mechanism to compensate for the constantly changing sun position. We hypothesize that this mechanism involves two distinct interaction sites between the circadian clock and the sun compass system. The first interaction ensures that all skylight information received by the sun compass system is consistent (elevation compensation), and the second interaction ensures that the animal flies in the correct direction, despite changing solar azimuth positions over the course of the day (azimuth compensation). Azimuthal compensation probably occurs on the output side of the sun compass, after integrating information from both eyes. Flight simulator experiments have shown that the antennae of the monarch are the location of the clock needed for azimuth compensation (Merlin et al., 2009) and defining a neural circuit from the antennae to the sun compass system is under investigation (Reppert et al., 2010). Elevation compensation, on the other hand, involves a clock interaction near the sensory periphery of the sun compass system, as this process is already apparent in the recorded TuLAL1 and TL neurons, which provide input to the sun compass. Thus, brain clock-derived, CRYPTOCHROME1-positive fibers in the monarch accessory medulla may mediate this interaction, because of their close proximity to photoreceptor input from the DRA (Sauman et al., 2005). These two forms of compensation, though interrelated, are distinct, because migrating monarchs can use the solar azimuth alone, independent of *E*-vector tuning and solar elevation, for appropriately time-compensated directional flight (Stalleicken et al., 2005). Further studies in the monarch will focus on the precise anatomical and functional interface of each of these two identified forms of clock-compass interactions.

In a broader context, the complex integration of different skylight cues in insects is an example of how ambiguous aspects of the sensory environment are integrated into a coherent neuronal representation of the outside world. The fundamental problem of disambiguation occurs across all sensory modalities and across all species, including humans. Our work highlights the power of the comparative approach, using insects as model systems, for unraveling such fundamental neural mechanisms.

EXPERIMENTAL PROCEDURES

Animals

Migrating monarch butterflies were captured in the wild from roosts between October 29 and 31, 2009 (for details see Supplemental Experimental Procedures for this and all other experimental sections). They were kept in the laboratory in glassine envelopes in Percival incubators with controlled light and temperature cycles imitating fall conditions (11 hr light:13 hr dark; light, 23°C:dark, 12°C) at 70% humidity. They were fed a 25% honey solution every other day. As monarch butterflies migrate during the daytime, recordings in migrants were performed around ZT 5, the midpoint of their normal flight time (from November 3, 2009 until March 2, 2010). Nonmigratory, summer monarch butterflies obtained from Fred Gagnon (Greenfield, Massachusetts) were used for initial recordings and the control experiments in Figure S2. These animals were also housed as described above but maintained in a 12 hr light:12 hr dark cycle at 25°C.

Immunocytochemistry

For immunocytochemical labeling of neuropils the brains were dissected out of the animal in physiological saline. After fixation in 4% paraformaldehyde/0.1 M phosphate buffer for 3 hr at room temperature, brains were rinsed in 0.1 M phosphate buffered saline (PBS). The ganglionic sheath was made permeable by treatment with 1 mg/ml collagenase-dispase (in PBS) for 1 hr. The brains were preincubated overnight with 5% normal goat serum (NGS) in PBS containing 0.3% Triton X (PBT) at 4°C. Next, the brains were incubated with a monoclonal antibody against the synaptic protein synapsin (dilution 1:50 in PBT) for 5 days at 4°C. The secondary antibody (Cy5-conjugated goat anti mouse; 1:300 in PBT) was applied for 3 days at 4°C. Finally, the brains were dehydrated in an increasing ethanol series, cleared with methyl salicylate, and mounted between two glass coverslides separated by spacing rings to avoid squeezing.

Image Acquisition and Three-Dimensional Neuropil Reconstructions

Confocal image stacks were obtained either with a 10× air objective or with a 25× oil-immersion objective. Low-resolution images (10×; final voxel size: 3 μm^3) were used for reconstruction of the complete brain, while high-resolution stacks were used for reconstruction of the central complex (25×; final voxel size 1 μm^3).

For reconstruction, neuropil areas of interest were manually labeled in Amira 5.0. Hereby, selected voxels were assigned to particular neuropils, resulting in a volumetric data set called the label field. The reconstruction of polygonal surface models was then automatically achieved on the basis of these label fields.

Histology for Neurobiotin Injections

After injection of Neurobiotin, brains were dissected out of the head capsule and fixed overnight at 4°C in Neurobiotin fixative (4% paraformaldehyde, 0.25% glutaraldehyde, 2% saturated picric acid, in 0.1 M phosphate buffer). After rinsing in PBS the brains were incubated with Cy3-conjugated Streptavidin (1:1000) for 3 days at 4°C. Finally, the brains were dehydrated in an increasing ethanol series, cleared in methylsalicylate, and mounted between two coverslides.

Neuron Reconstruction

All reconstructions of single neurons were based on neurobiotin injected cells. Confocal image stacks were acquired with the 25× objective. For two-dimensional neuron reconstructions, image stacks were loaded into Photoshop software and arborizations were traced with the pencil tool. According to neuropil boundaries visible from background staining, the resulting image was finally projected onto a three-dimensional reconstruction of the central-complex neuropils. Three-dimensional reconstructions of neurons were achieved by using a supplemental tool for Amira 4.2 as described by Schmitt et al. (2004). The updated version of this tool was kindly provided by J.F. Evers (Cambridge, UK). For obtaining neuropil reconstructions from the dye-injected brains, unspecific background staining was used analogous to anti-synapsin staining.

Electrophysiology

For recordings, animals were waxed onto a plastic holder. Legs and wings were removed and the head capsule was opened frontodorsally. Recordings were all performed on the left side of the brain. For accessing the recording site, the left antenna was removed, while the right antenna was left intact; behavioral studies in a flight simulator have shown that one antenna is sufficient for proper time-compensated sun compass orientation (P.A. Guerra and S.M.R., unpublished data). To increase stability, the oesophagus was transected and the gut was removed from the opened abdomen. The neural sheath was locally removed mechanically with forceps after brief enzymatic digestion and intense rinsing with ringer solution (150 mM NaCl, 3 mM KCl, 10 mM TES, 25 mM sucrose, 3 mM $CaCl_2$; pH = 6.9; King et al., 2000). The animal was then mounted in the recording setup, with the vertical axis of the

compound eye aligned horizontally. Thus the dorsal side of the eye faced the stimulation setup, while the recording electrode could be inserted vertically from the frontal side.

Intracellular recordings were performed with sharp electrodes (resistance 60–150 MΩ), drawn from borosilicate capillaries. Electrode tips were filled with 4% Neurobiotin dissolved in 1 M KCl and backed up with 1 M KCl. Intracellular signals were amplified (10×) with a SEC05-LX amplifier (NPI), digitized, and stored on a PC (details in Supplemental Experimental Procedures). After applying all stimuli, depolarizing current was applied (1–3 nA, 1–5 min) to iontophoretically inject Neurobiotin when stability of recording allowed.

Visual Stimulations

Two different types of visual stimuli were applied during the experiments. First, linearly polarized light was presented from the zenith (as seen by the animal). Second, unpolarized light spots were presented at an elevation of 25°–30° (above the animal's horizon). Both stimuli were connected to a rotation stage, which could be rotated by 360° in either direction. Through a central hole in the rotation stage, light from a light-emitting diode (LED, ultraviolet, 365 nm emission peak) was passed via a polarization filter (angular size: 19°). During each rotation the plane of polarization was rotated by 360° (0° defined as the *E*-vector parallel to the longitudinal body axis of the animal). The LEDs for unpolarized stimulation (ultraviolet [365 nm], green [520 nm], blue [460 nm]) were attached to the rotation stage via radial arms extending from the zenith, so that each LED pointed toward the animal (angular size: 3°). With every rotation, each LED passed through all possible azimuth directions at constant elevation. Photon flux rate was equal for all unpolarized stimuli. Over the course of experiments, rotation velocity was either set to 30°/s or 60°/s, and both clockwise as well as counterclockwise rotations were applied in direct sequence.

For blocking light to the dorsal region of the compound eye, a small piece of black tape was positioned directly in front of the eye. Identical stimuli were applied before, during, and after the shielding.

For eliminating polarization during control experiments with zenithal unpolarized light, a diffuser was inserted into the light path. Residual polarization during 360° rotations of the polarizer/diffuser was found to be below 5%. Intensity of polarized light was adjusted to match the unpolarized light intensity resulting from insertion of the diffuser.

Analysis of Electrophysiological Data

Neuronal responses to rotations of the polarizer as well as to azimuthal rotations of unpolarized light spots were analyzed with custom designed scripts in Spike2 software. Each spike occurring during a rotation was assigned its corresponding angle (either *E*-Vector or azimuth). These angles were tested for significant difference from randomness using the Rayleigh test for axial (*E*-vector angles) or circular data (azimuth angles). If activity during rotations was significantly different from randomness, the resulting mean angle was defined as the preferred *E*-vector or azimuth angle of the examined neuron. For circular plots, spiking activity during rotations was calculated for 10° bins, averaged over all rotations within each neuron, and plotted against *E*-vector orientation or azimuth angle, respectively.

The response amplitude (R) was calculated as described in Heinze et al. (2009). In brief, R is a measure for the summed absolute deviation from mean activity during stimulus application. Thus, the higher the value of R, the stronger is the response to the stimulus. R values for periods without stimulation were obtained to calculate background variability.

Statistical comparison between shielded and unshielded stimulus conditions were performed by analyzing R values for each of the conditions. After R values were normalized to the unshielded response value, a paired t test was then used to compare the shielded response to background variability while a one-sample t test against a hypothetical mean of 1 was performed to compare the shielded response against the normalized unshielded response.

Distributions of preferred tuning directions (*E*-vector or azimuth tunings) were compared with the Watson-Williams F test or the Watson U^2 test. Significant deviation from randomness of each population of tunings was tested with the Rayleigh test. Mean azimuth tunings were calculated by averaging individual color tunings (circular mean ± SD). The difference angle between *E*-vector tuning and mean azimuth tuning was defined as the absolute value of the smaller of the two difference angles (resulting range: 90°). The difference angles between responses to individual colors were defined analogous (resulting range: 180°). Finally, the distributions of difference angles were tested for significant deviations from a uniform distribution with the Kuiper's V test.

Modeling

Skylight features of the relevant part of the sky were calculated by using the single-scattering Rayleigh model (Coulson, 1988), following the implementation by Pfeiffer et al. (2011) and Pfeiffer and Homberg (2007).

For determining the skylight parameters available to the monarch, the degree of polarization (d) and the *E*-vector angle (Φ) were calculated for different elevations along the 90° azimuth (in steps of 10°, between 20° and 90° elevation). First, results for all possible solar elevations were calculated (resolution 1°; Figures S2C and S2D). Next, the average *E*-vector angle (Φ_{mean}) across the observed region was determined for any given solar elevation. Hereby, d^4 was used as a weighing factor in order to eliminate degrees of polarization less than 30% (Figure S3).

After Φ_{mean} was calculated for each possible solar elevation, its value was determined for different solar elevations over the course of the day at the capture sites (at date of capture) of the used butterflies. The time of sunrise was set to ZT0.

The predictions made by the model are viable if three assumptions are met. First, all neurons must have an identical, contralaterally centered azimuth tuning as suggested by our data. For neurons with different azimuth tunings, the area viewed by the DRA at Φ_{max} does not coincide with the 90° azimuth and the derived equations do not fully apply (see Supplemental Experimental Procedures). Second, monarch butterflies should not be able to use degrees of polarization of less than 30%. This value was chosen to match the capability of the desert locust (Pfeiffer et al., 2011), as it is the only other long-distance migrant examined in this regard. Third, the information coded by the recorded neurons must be integrated over the complete DRA, as the predicted *E*-vector is the average perceived *E*-vector across the DRA. Receptive fields covering the whole DRA have been shown at early stage POL neurons from the optic lobe in the cricket (Labhart et al., 2001). The trend toward large receptive fields was also observed in polarization sensitive neurons from the locust (Heinze et al., 2009).

SUPPLEMENTAL INFORMATION

Supplemental Information includes five figures and Supplemental Experimental Procedures and can be found with this article online at doi:10.1016/j.neuron.2010.12.025.

ACKNOWLEDGMENTS

We kindly thank David G. Cook of the St. Marks National Wildlife Refuge (St. Marks, Florida) and Harlen E. Aschen and Altus Aschen for providing migratory butterflies; Lauren Foley, Daniel Newman, and Andrea Pereira for animal care; Keram Pfeiffer for providing Spike2 scripts for data analysis; Eugenia Chiappe and Vivek Jayaraman for assistance with equipment for stimulus delivery; Robert Gegear for assistance with statistical analysis; the UMASS machine shop for building custom-designed equipment; Jan-Felix Evers for providing an updated version of the skeletonize tool for neuron reconstruction in Amira4.2; and members of the Reppert lab for discussions and comments on various parts of the manuscript. This work was supported by AFOSR grant FA9550-10-1-0480. S.H. was supported by a long-term fellowship from the Human Frontier Science Program (LT000379/2009-L); the funders had no role in study design, data collection, and analysis, decision to publish, or preparation of the manuscript.

Accepted: October 21, 2010
Published: January 26, 2011

REFERENCES

Coemans, M.A., Vos Hzn, J.J., and Nuboer, J.F. (1994). The relation between celestial colour gradients and the position of the sun, with regard to the sun compass. Vision Res. *34*, 1461–1470.

Coulson, K.L. (1988). Polarization and Intensity of Light in the Atmosphere (Hampton: A. Deepak Publishing).

El Jundi, B., Huetteroth, W., Kurylas, A.E., and Schachtner, J. (2009). Anisometric brain dimorphism revisited: Implementation of a volumetric 3D standard brain in *Manduca sexta*. J. Comp. Neurol. *517*, 210–225.

Froy, O., Gotter, A.L., Casselman, A.L., and Reppert, S.M. (2003). Illuminating the circadian clock in monarch butterfly migration. Science *300*, 1303–1305.

Gaunt, M.W., and Miles, M.A. (2002). An insect molecular clock dates the origin of the insects and accords with palaeontological and biogeographic landmarks. Mol. Biol. Evol. *19*, 748–761.

Heinze, S., and Homberg, U. (2007). Maplike representation of celestial *E*-vector orientations in the brain of an insect. Science *315*, 995–997.

Heinze, S., and Homberg, U. (2008). Neuroarchitecture of the central complex of the desert locust: Intrinsic and columnar neurons. J. Comp. Neurol. *511*, 454–478.

Heinze, S., and Homberg, U. (2009). Linking the input to the output: New sets of neurons complement the polarization vision network in the locust central complex. J. Neurosci. *29*, 4911–4921.

Heinze, S., Gotthardt, S., and Homberg, U. (2009). Transformation of polarized light information in the central complex of the locust. J. Neurosci. *29*, 11783–11793.

Homberg, U. (2004). In search of the sky compass in the insect brain. Naturwissenschaften *91*, 199–208.

Homberg, U., and Paech, A. (2002). Ultrastructure and orientation of ommatidia in the dorsal rim area of the locust compound eye. Arthropod Struct. Dev. *30*, 271–280.

Homberg, U., Hofer, S., Pfeiffer, K., and Gebhardt, S. (2003). Organization and neural connections of the anterior optic tubercle in the brain of the locust, *Schistocerca gregaria*. J. Comp. Neurol. *462*, 415–430.

Kelber, A. (1999). Why 'false' colours are seen by butterflies. Nature *402*, 251.

King, J.R., Christensen, T.A., and Hildebrand, J.G. (2000). Response characteristics of an identified, sexually dimorphic olfactory glomerulus. J. Neurosci. *20*, 2391–2399.

Kinoshita, M., Pfeiffer, K., and Homberg, U. (2007). Spectral properties of identified polarized-light sensitive interneurons in the brain of the desert locust *Schistocerca gregaria*. J. Exp. Biol. *210*, 1350–1361.

Labhart, T. (1999). How polarization-sensitive interneurones of crickets see the polarization pattern of the sky: A field study with an opto-electronic model neurone. J. Exp. Biol. *202*, 757–770.

Labhart, T., and Meyer, E.P. (1999). Detectors for polarized skylight in insects: A survey of ommatidial specializations in the dorsal rim area of the compound eye. Microsc. Res. Tech. *47*, 368–379.

Labhart, T., Petzold, J., and Helbling, H. (2001). Spatial integration in polarization-sensitive interneurones of crickets: A survey of evidence, mechanisms and benefits. J. Exp. Biol. *204*, 2423–2430.

Labhart, T., Baumann, F., and Bernard, G.D. (2009). Specialized ommatidia of the polarization-sensitive dorsal rim area in the eye of monarch butterflies have non-functional reflecting tapeta. Cell Tissue Res. *338*, 391–400.

Merlin, C., Gegear, R.J., and Reppert, S.M. (2009). Antennal circadian clocks coordinate sun compass orientation in migratory monarch butterflies. Science *325*, 1700–1704.

Mouritsen, H., and Frost, B.J. (2002). Virtual migration in tethered flying monarch butterflies reveals their orientation mechanisms. Proc. Natl. Acad. Sci. USA *99*, 10162–10166.

Müller, M., Homberg, U., and Kühn, A. (1997). Neuroarchitecture of the lower division of the central body in the brain of the locust (*Schistocerca gregaria*). Cell Tissue Res. *288*, 159–176.

Perez, S.M., Taylor, O.R., and Jander, R. (1997). A sun compass in monarch butterflies. Nature *387*, 29.

Pfeiffer, K., and Homberg, U. (2007). Coding of azimuthal directions via time-compensated combination of celestial compass cues. Curr. Biol. *17*, 960–965.

Pfeiffer, K., Kinoshita, M., and Homberg, U. (2005). Polarization-sensitive and light-sensitive neurons in two parallel pathways passing through the anterior optic tubercle in the locust brain. J. Neurophysiol. *94*, 3903–3915.

Pfeiffer, K., Negrello, M., and Homberg, U. (2011). Conditional perception under stimulus ambiguity: Polarization- and azimuth-sensitive neurons in the locust brain are inhibited by low degrees of polarization. J. Neurophysiol. *105*, 28–35.

Reppert, S.M. (2007). The ancestral circadian clock of monarch butterflies: Role in time-compensated sun compass orientation. Cold Spring Harb. Symp. Quant. Biol. *72*, 113–118.

Reppert, S.M., Zhu, H., and White, R.H. (2004). Polarized light helps monarch butterflies navigate. Curr. Biol. *14*, 155–158.

Reppert, S.M., Gegear, R.J., and Merlin, C. (2010). Navigational mechanisms of migrating monarch butterflies. Trends Neurosci. *33*, 399–406.

Rossel, S., Wehner, R., and Lindauer, M. (1978). E-vector orientation in bees. J. Comp. Physiol. A Neuroethol. Sens. Neural Behav. Physiol. *125*, 1–12.

Sakura, M., Lambrinos, D., and Labhart, T. (2008). Polarized skylight navigation in insects: Model and electrophysiology of e-vector coding by neurons in the central complex. J. Neurophysiol. *99*, 667–682.

Sauman, I., Briscoe, A.D., Zhu, H., Shi, D., Froy, O., Stalleicken, J., Yuan, Q., Casselman, A., and Reppert, S.M. (2005). Connecting the navigational clock to sun compass input in monarch butterfly brain. Neuron *46*, 457–467.

Schmitt, S., Evers, J.F., Duch, C., Scholz, M., and Obermayer, K. (2004). New methods for the computer-assisted 3-D reconstruction of neurons from confocal image stacks. Neuroimage *23*, 1283–1298.

Stalleicken, J., Mukhida, M., Labhart, T., Wehner, R., Frost, B., and Mouritsen, H. (2005). Do monarch butterflies use polarized skylight for migratory orientation? J. Exp. Biol. *208*, 2399–2408.

Stalleicken, J., Labhart, T., and Mouritsen, H. (2006). Physiological characterization of the compound eye in monarch butterflies with focus on the dorsal rim area. J. Comp. Physiol. A Neuroethol. Sens. Neural Behav. Physiol. *192*, 321–331.

Träger, U., Wagner, R., Bausenwein, B., and Homberg, U. (2008). A novel type of microglomerular synaptic complex in the polarization vision pathway of the locust brain. J. Comp. Neurol. *506*, 288–300.

Vitzthum, H., Müller, M., and Homberg, U. (2002). Neurons of the central complex of the locust *Schistocerca gregaria* are sensitive to polarized light. J. Neurosci. *22*, 1114–1125.

Wehner, R. (1982). Himmelsnavigation bei Insekten: Neurobiologie und Verhalten. Neujahrsbl. Naturforschende. Ges. Zürich *182*, 1–132.

Wehner, R. (2001). Polarization vision—a uniform sensory capacity? J. Exp. Biol. *204*, 2589–2596.

Wehner, R., and Labhart, T. (2006). Polarization vision. In Invertebrate Vison, E. Warrant and D.-E. Nilsson, eds. (Cambridge, UK: Cambridge Univ. Press), pp. 291–348.

Zhu, H., Gegear, R.J., Casselman, A., Kanginakudru, S., and Reppert, S.M. (2009). Defining behavioral and molecular differences between summer and migratory monarch butterflies. BMC Biol. *7*, 14.